Geophysical Research Letters

RESEARCH LETTER

10.1029/2021GL092997

Key Points:

- Industrial heat sources in China are identified by Visible Infrared Imaging Radiometer Suite (VIIRS) thermal anomaly products
- VIIRS fire radiative power has high correlations with industrial emission
- VIIRS thermal detection can provide dynamic constraint on industrial emission estimates and spatial allocation

Supporting Information:

Supporting Information may be found in the online version of this article.

Correspondence to:

M. Tao,
taomh@cug.edu.cn

Citation:

Li, R., Tao, M., Zhang, M., Chen, L., Wang, L., Wang, Y., et al. (2021). Application potential of satellite thermal anomaly products in updating industrial emission inventory of China. *Geophysical Research Letters*, *48*, e2021GL092997. https://doi.org/10.1029/2021GL092997

Received 16 FEB 2021
Accepted 11 APR 2021

Application Potential of Satellite Thermal Anomaly Products in Updating Industrial Emission Inventory of China

Rong Li[1,2], Minghui Tao[3], Meigen Zhang[4], Liangfu Chen[5], Lili Wang[4], Yi Wang[6,7], Xinjie He[1], Lifei Wei[1,2], Xin Mei[1,2], and Jun Wang[6,7]

[1]Faculty of Resources and Environmental Science, Hubei University, Wuhan, China, [2]Hubei Key Laboratory of Regional Development and Environmental Response, Hubei University, Wuhan, China, [3]Hubei Key Laboratory of Critical Zone Evolution, School of Geography and Information Engineering, China University of Geosciences, Wuhan, China, [4]State Key Laboratory of Atmospheric Boundary Layer Physics and Atmospheric Chemistry, Institute of Atmospheric Physics, Chinese Academy of Sciences, Beijing, China, [5]State Key Laboratory of Remote Sensing Science, Aerospace Information Research Institute, Chinese Academy of Sciences, Beijing, China, [6]Department of Chemical & Biochemical Engineering, The University of Iowa, Iowa City, IA, USA, [7]Center for Global and Regional Environmental Research, The University of Iowa, Iowa City, IA, USA

Abstract Establishing dynamic and timely industrial emissions inventory accurately is usually challenging due to a long update cycle of the time-consuming bottom-up methods. The daily Visible Infrared Imaging Radiometer Suite (VIIRS) thermal anomaly product at a high resolution of 375 m can detect spatial location and fire radiative power (FRP) of thermal anomalies including industrial heat sources. We explore potential of VIIRS product in updating industrial emission inventory. Industrial heat sources in China are identified and further compared with industrial emissions from Multi-resolution Emission Inventory for China. The correlations (R^2) between VIIRS FRP and industrial emissions are 0.86 in regions dominated by coal-consuming activities and 0.9 for these with fragmented small-scale plants and light industries. Our results suggest that VIIRS thermal product can provide a dynamic and quantitative constraint of activation levels and spatial allocation of emission from industrial heat sources.

Plain Language Summary The combustion of fossil fuels in global industrial activities emits a large amount of atmospheric pollutants and greenhouse gases every year, which is considered as the main anthropogenic factor causing air pollution and climate change. Owing to a comprehensive estimation of the diverse industrial emissions, bottom-up methods usually have a time-consuming compilation process for years. Satellites provide near-real-time observations of atmospheric composition, which are useful constraints for updating emissions inventories timely. However, there are only several satellite products of atmospheric components with reliable accuracy by now. In this study, we present a probing insight into the application potential of Visible Infrared Imaging Radiometer Suite (VIIRS) thermal anomaly product with a high resolution of 375 m for updating industrial emissions inventory of China. Comparison of VIIRS fire radiative power (FRP) in industrial heat sources and Multi-resolution Emission Inventory for China industry emission shows similar spatial patterns for both their location and magnitude. By analyzing the correlation of satellite FRP and emission inventory, our results suggest that the high-resolution satellite thermal anomaly product can provides a dynamic and quantitative constrain for industry emission levels and reallocation of industrial heat sources

1. Introduction

Combustion of fossil fuels in global industrial activities emits large amounts of atmospheric pollutants and greenhouse gases every year, which is considered as the main anthropogenic factor in air pollution and climate change (Guo et al., 2019; Krotkov et al., 2016; Oberschelp et al., 2019). During the last decades, industrial emissions of atmospheric pollutants in China have experienced dramatic changes due to both fast-growing economy and strict control measures (Li et al., 2020; Tao et al., 2020; Zheng et al., 2018). As an essential input of air quality and climate models, accurately quantifying emissions of industrial activities is fundamental in understanding the changing climate and air quality. However, the diverse industrial sources as well as their activity levels usually have large spatial and temporal variations, leading to a requirement of timely and dynamic emission inventory.

Based on statistical industrial activity rates and emissions factors, emission inventory developed by bottom-up methods has been widely used in atmospheric chemistry and climate studies (Streets et al., 2003; Zhang et al., 2009). Comprehensive estimation of complicated industrial emissions with bottom-up methods in large scales such as China has a time-consuming compilation process for years and is subject to substantial uncertainties due to limited knowledge of emission factors, activation levels, and spatial allocation (Li et al., 2017; Zhao et al., 2011). Satellite observations of atmospheric composition can provide a dynamic and timely constraint for updating emissions inventories. Advanced approaches including four-dimensional variational data assimilation and Ensemble Kalman Filter utilize satellite products such as SO_2 and NO_2 vertical column density to update corresponding emissions inventory in monthly scales (Qu et al., 2017; Y. Wang et al., 2016, 2020). However, there are only several satellite products of atmospheric components with reliable accuracy by now. Additionally, these satellite-based emission estimates are only the total amount rather than source-resolved, hence lacking information for spatial and temporal variations of industrial activities.

The energy-consuming industrial activities always release intense heat accompanied by high temperatures, which can be quantitatively detected by satellite thermal infrared observations. Recent Visible Infrared Imaging Radiometer (VIIRS) thermal anomaly products can not only provide location and Fire Radiation Power (FRP) of biomass burning fires (Schroeder et al., 2014), but are also very sensitive to large industrial heat sources due to a high spatial resolution at 375 m (Liu et al., 2018; Zhang et al., 2019). The industrial hotspots identified by daily satellite detection enable valuable spatial and temporal information of regional industrial activities required in timely and dynamic emissions inventory. However, the few existing studies mostly focus on identification methods and spatial patterns of the industrial hotspots. VIIRS thermal radiation has been found an effective indicator for emissions of fuel combustion such as flared gas volume (Franklin et al., 2019). Besides spatial location, to what extent can satellite thermal observations characterize industrial emissions remain unclear by now.

In this study, we explore the application potential of satellite thermal anomaly in characterizing industrial emissions based on VIIRS products and emission inventory in China. The industrial heat sources are identified by VIIRS 375 m product combined with land cover data at 30 m. Then, a density-based clustering method is used to exclude the noisy points and extract industrial objects. Section 2 introduces data and methods used. The relationship among VIIRS FRP, industrial emissions and energy consumption is analyzed in section 3. The limitation and uncertainty of satellite thermal products in emission inventory are also discussed. Additionally, a summary is given in Section 4.

2. Data and Methods

2.1. VIIRS Fire and Thermal Anomaly Product

The day and night VIIRS 375 m active fire product from NASA is used to identify industrial heat sources. After screening out cloud and water pixels, VIIRS fire algorithm detects thermal anomalies (e.g., wildfire, agricultural biomass burning, and industrial activities) by brightness temperature at middle and thermal infrared bands using a contextual approach (Schroeder et al., 2014). Besides location of the fires, FRP indicating the rates of fire radiative energy related directly with combustion and emission process is also calculated at pixel level. Additionally, each fire pixel is labeled with a confidence flag (low, nominal, or high). There are a total of 465,422 thermal anomaly pixels of nominal or high confidence during 2016 in China.

2.2. Land Cover Data

Considering that satellite infrared observations do not have information regarding source types of the thermal anomalies, a high-resolution global land cover data set at 30 m, GlobeLand30, is selected to distinguish industrial heat sources to biomass burning fires (http://www.globallandcover.com/). By merging satellite images from Landsat and China Environmental Disaster Alleviation Satellite, GlobeLand30 has 10 types of land covers with an overall classification accuracy of 85.72% (Chen et al., 2014). The artificial surfaces at a high spatial resolution can effectively separate industrial heat sources from all other thermal anomaly points (Figure S1). Owing to the narrow swath width and cloud cover, GlobeLand30 is available for the year of 2000, 2010, 2020, and we utilize the 2020 version here.

2.3. Industrial Emissions Inventory and Energy Consumption Statistics

The Multi-resolution Emission Inventory for China (MEIC) anthropogenic emission inventory in 2016 at 0.25° × 0.25° is used to examine the potential of VIIRS thermal anomaly in emissions estimates (Li et al., 2017). MEIC consists of 10 pollutants including SO_2, NOx, CO, NMVOC, NH_3, CO_2, $PM_{2.5}$, PM_{10}, BC, and OC emitted from five sectors of industry, agriculture, power plants, residential, and transportation. Since industrial heat sources include several types such as power plants, steel plants, and cement plants, we aggregate MEIC emissions of the 10 pollutants emitted from industry and power plant sectors to make a comparison. To inspect the relationship between FRP of industrial heat sources and the amount of energy consumption, we collect the provincial coal and fuel consumption in 2016 from national statistical yearbooks (http://www.stats.gov.cn/tjsj/).

2.4. Cluster Analysis and FRP Aggregation of the Industrial Heat Sources

Unlike the sporadic biomass burning fires, industrial heat sources are fixed and persistent in a small area and a long-time window such as 1 year. However, one large industrial hotspot usually has several striking heat sources, and even location of the same hear source can be influenced by changing pixel sizes due to daily variations of VIIRS orbit. The Density-based Spatial Clustering of Applications with Noise (DBSCAN) algorithm can cluster points such as industrial heat sources in a region of specified radius according to their density (Ester et al., 1996). To extract the industrial hotspots, we cluster VIIRS thermal anomaly pixels in artificial surfaces of GlobeLand30 by an improved DBSCAN, which can not only consider spatial and temporal attributes of the data set, but also detect the noise points from clusters of different densities (Birant & Kut, 2007). High-resolution Google Earth images are used to confirm industrial hotspots and heat sources further visually. To deal with the influence of cloud cover, monthly or annual mean of daily VIIRS FRP is calculated at 375 m to indicate activity level of industrial emissions. Then, these unified FRP of the industrial heat sources are accumulated into 0.25° × 0.25°grids to match with MEIC.

3. Results and Discussion

3.1. Identification of Industrial Heat Sources in Mainland China

During 2016, 43.8% (204,058) of the VIIRS thermal anomalies in China are located in artificial surfaces of GlobeLand30, which are taken as candidates of industrial heat sources. By confirmation in Google Earth images, these thermal anomalies can be caused by typical industrial activities such as cement plants, coal-fired power plants, steel plants, and coal mines (Figures 1a–1d). However, some thermal anomaly points are found in residential area and construction site due to non-industrial sources like heating in winter and open burning (Figures 1e and 1f). It should be noting that the dense thermal anomaly points in coal mines and steel plants mainly result from different pixel sizes or center locations of the pixels due to daily shift of VIIRS orbit.

To eliminate the influence of VIIRS orbit shift and filter out the noise ones, DBSCAN algorithm is applied to cluster the candidates of industrial heat sources. Similar as previous work (Liu et al., 2018), radius of the clustering is set to 1 km and the minimum number of the points within the radius is 5. After removing 14,190 noise points, 2,238 industrial objects are extracted from the 189,868 candidate points. Considering that false thermal anomalies can exist in small towns surrounded by croplands or forest in contextual algorithm (Schroeder et al., 2014), we verify all the industrial objects through visually comparation with high-resolution image of Google Earth manually. There are 2,055 high-confidence industrial heat sources identified, which is close to the result (2,491) from Liu et al. (2018) but much fewer than that (16,505 polygons) by Zhang et al. (2019). The large difference could be due to that thermal anomaly points in a large-area factory is divide into several polygons by the three-sliding window algorithm used in Zhang et al. (2019).

10.1029/2021GL092997

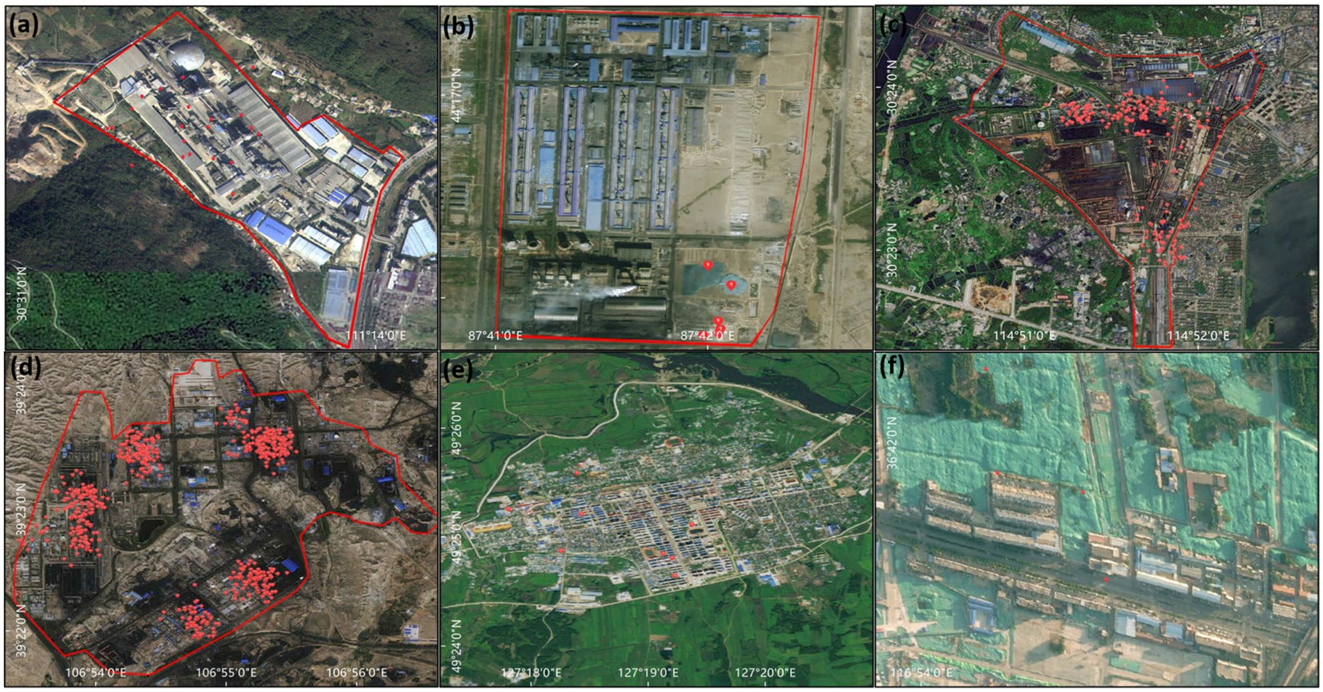

Figure 1. Typical industrial heat sources including (a) cement plant, (b) coal-fired power plant, (c) steal plant, (d) coal mine, and noise points (e)–(f) viewed from Google earth images.

Figure 2 shows spatial patterns of the 2,055 industrial heat sources clustering from 188,322 VIIRS high-confidence thermal anomaly points during 2016 (Figure 2). The large industrial heat sources are most concentrated in northern China and then the Yangtze River economic belt. Despite a much lower density, there are also numerous thermal anomaly points in industrial regions of northwestern China, where coal mines and oil-gas fields prevail. It is interesting that the industrial heat sources in Guangdong of southern China are scattered across the whole province rather than converge surrounding the megacity of Guangzhou, due to large evacuation of industrial sources in air quality improvement (Z. Wang et al., 2016).

3.2. Comparison of VIIRS FRP and MEIC Emissions of Industrial Heat Sources

To have a direct view of satellite thermal detection in characterizing industrial activities, unified VIIRS FRP aggregated at $0.25° \times 0.25°$ is compared with MEIC industrial emissions in mainland China during 2016. As shown in Figure 3, there is a high consistency in spatial patterns of VIIRS FRP and MEIC industrial emissions. The MEIC industrial emission hotspots in northern and northwestern China have notable high FRP values (seen in the red circles). However, the striking emission hotspot in Guangzhou of southern China exhibits few thermal anomaly points and high values of FRP, which can be caused by industrial structures and uncertainties of emission inventory. Also, it should be noted that there are numerous spatial discrepancies in the detailed location of the high values of VIIRS FRP and MEIC industrial emissions. While high values of MEIC industrial emissions exhibit very concentrated distribution, those of VIIRS FRP are more scattered.

Although spatial locations of high values of VIIRS FRP and MEIC industrial emissions are not exactly matched, their locations in the same industrial hotspot tend to be close with each other (Figure 3). Spatial allocation of emissions from nonpoint sources of industrial sectors usually adopts population-based method (Li et al., 2017), which can miss the small scattered industrial sources and allocate more emissions to the central urban areas. Compared with the concentrated heavy industries such as steel plants and coal-fired plants in northern China, the fragmented FRP values at moderate levels in southern China demonstrate different industrial emission structures at much smaller scales. Moreover, spatial discrepancies between VIIRS FRP and MEIC industrial emissions are obviously larger in southern China.

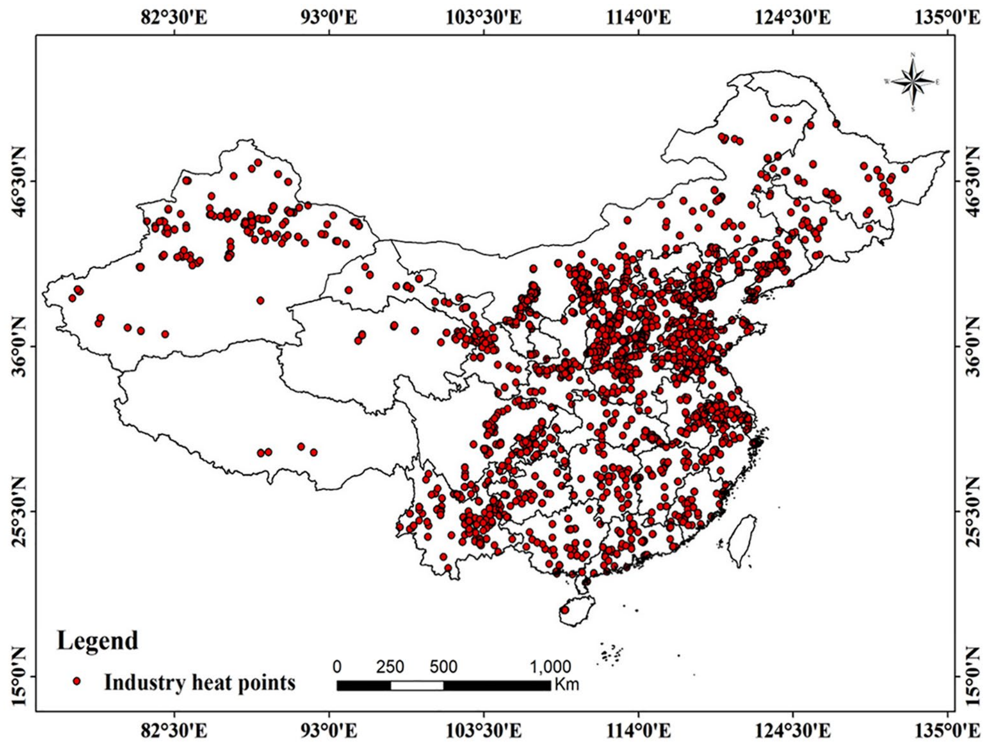

Figure 2. Distribution of high-confidence industrial heat sources in China during 2016.

Owing to the prominent spatial mismatch, we analyze correlation of unified VIIRS FRP with MEIC industrial emissions and energy consumption at provincial levels (Figure S2). VIIRS FRP agrees well with industrial emissions and the amount of energy consumption with coefficient of determination (R^2) of 0.63 and 0.73, respectively. Their total amounts at provincial levels can partly offset the influence of spatial mismatch in the correlation. On the other hand, their direct correlation can also be hindered by distinct industrial structures in different regions.

3.3. Application Potential of VIIRS FRP in Industrial Emission Estimation

According to clustering feature in scatter plots representing VIIRS FRP, MEIC industrial emission, and energy consumption in different provinces (Figure S2), we find that these data points can be obviously divided into two groups (Figure 4). The slope of linear regression between FRP and industrial emission for group 1 (rectangle) is twice that for group 2 (circle), demonstrating different energy structures. Provinces in group 1 are mainly located in northwestern and southwestern China, as well as Shandong and Hebei, which are characterized by coal-fired heavy industries such as steel plants, power plants, and coal mines/oil-gas fields. By contrast, VIIRS FRP indicates those in group 2 is dominated by fragmented small-scale plants and light industries, with much weaker heat release and higher energy efficiency. Despite a simple grouping of the provinces, R^2 between FRP and industrial emissions or energy consumption increases largely from 0.63 to 0.86 and 0.9 or from 0.73 to 0.82 and 0.92.

Despite different slopes in the correlation, the point-to-point comparison of VIIRS FRP and MEIC industrial emissions in several typical provinces exhibits robust correlation at grid levels (Figure S3), proving that VIIRS FRP is a good proxy in industrial emission estimates. Cloud cover can reduce daily coverage of satellite detection, but unified VIIRS FRP at monthly scales is fully adequate for supporting emission inventory updating. Even so, unified VIIRS FRP can be more effective in characterizing variations of activation levels of industrial emissions at a high temporal resolution of monthly scale rather than their amount. Meanwhile, the high-resolution VIIRS 375 m thermal anomaly products can provide an observational constraint for spatial allocation of industrial emissions. In particular, VIIRS FRP can be utilized together with other satellite products such as trace gases in updating emission inventory (Y. Wang et al., 2016, 2020).

10.1029/2021GL092997

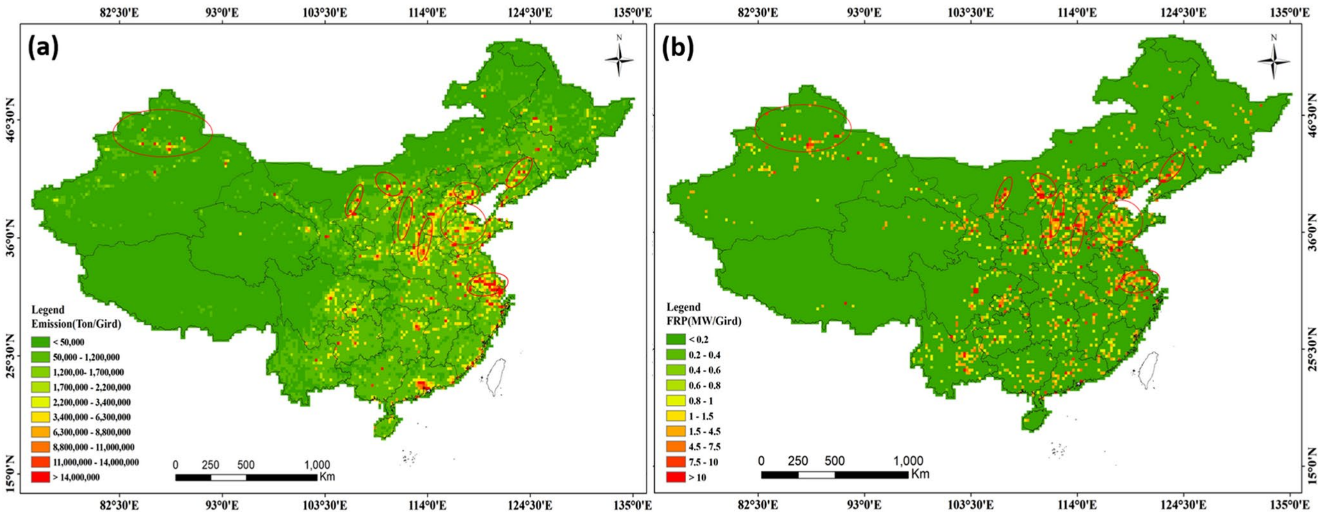

Figure 3. Comparison of MEC emissions (a) and unified VIIRS FRP (b) of industrial sources in China during 2016. FRP, fire radiative power; MEC, Multi-resolution Emission Inventory for China; VIIRS, Visible Infrared Imaging Radiometer Suite.

To promote emission inventory updating with VIIRS thermal anomaly products, several problems should be further considered. Since VIIRS FRP itself does not have information regarding specific types of the emission sources, how to deal with the numerous mismatches between FRP and emission inventory remains a challenge. Other satellite products of atmospheric components and priori knowledge such as pollutant concentration from air quality monitoring network in China and fieldworks can provide a lot of favors. In addition, the changing pixel size due to daily orbit shift or larger view angles can reduce the confidence of spatial location and FRP of the thermal anomaly.

4. Conclusions

The huge amounts of atmospheric pollutants from large-scale industrial activities in China have significant influence on regional air quality and climate changes. However, to update emission inventory of the dynamic industrial sources is a fundamental requirement but challenging work due to a time-consuming compilation process of the common bottom-up methods. Here, we present an exploratory insight into the

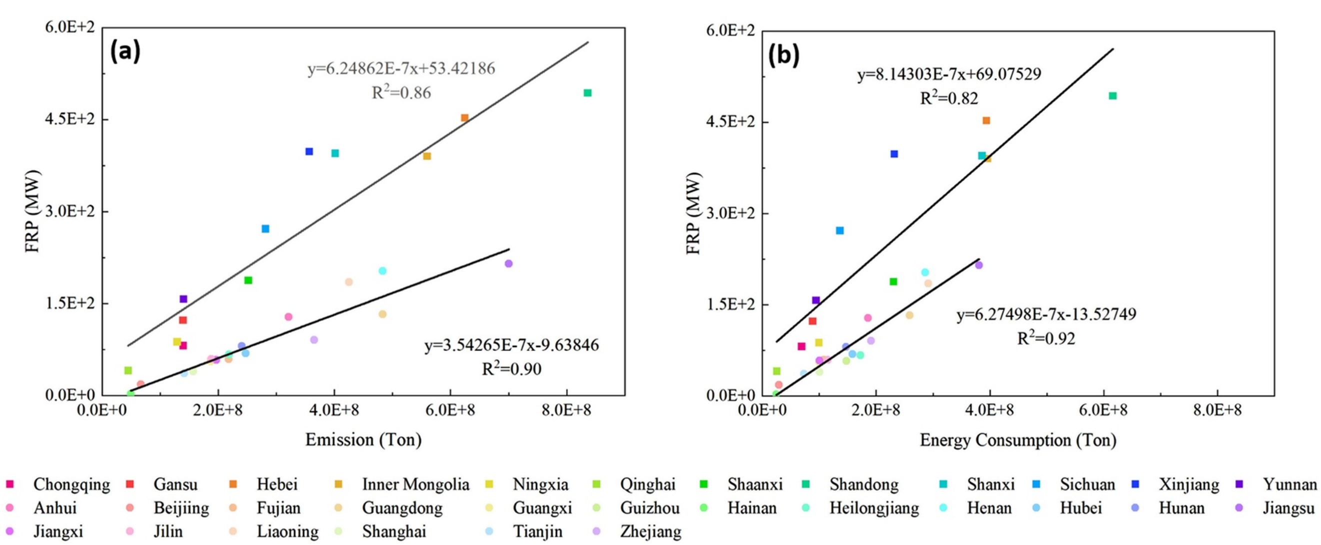

Figure 4. Linear regression between FRP and emissions (a) and that between FRP and energy consumption (b) in two regions of China during 2016. FRP, fire radiative power.

application potential of satellite thermal anomaly products in industrial emission estimates. Industrial heat sources in China are identified by VIIRS 375 m products with a density-based clustering algorithm. VIIRS FRP and MEIC industrial emission have very similar spatial patterns, but numerous mismatches exist in their detailed location. There is a robust correlation between FRP and industrial emissions at both provincial and grid levels. VIIRS thermal anomaly products prove to be a quantitative indicator of energy-consuming emissions and can be used in characterizing activation levels and spatial allocation of industrial emissions.

Data Availability Statement

The authors acknowledge the free use of VIIRS products (https://ladsweb.modaps.eosdis.nasa.gov/) and MEIC emissions data (http://www.meicmodel.org/).

Acknowledgments

This work was supported by the National Natural Science Foundation of China (Grant No. 41871262 and 41830109), Foundation of Hubei University (Grant No. 201910804000002), and the Open Foundation of regional development and environment in Hubei Province (Grant No. 2019(B)003).

References

Birant, D., & Kut, A. (2007). ST-DBSCAN: An algorithm for clustering spatial-temporal data. *Data & Knowledge Engineering*, *60*, 208–221. https://doi.org/10.1016/j.datak.2006.01.013

Chen, J., Ban, Y., & Li, S. (2014). China: Open acess to Earth land-cover map. *Nature*, *514*(7523).

Ester, M., Kriegel, H., Sander, J., & Xu, X. (1996). A density-based algorithm for discovering cluster in large spatial database with noise. In *Proceeding 2nd international conference On knowledge discovery and data mining* (pp. 226–231). California (USA).

Franklin, M., Chau, K., Cushing, L. J., & Johnston, J. E. (2019). Characterizing flaring from unconventional oil and gas operations in south Texas using satellite observations. *Environmental Science & Technology*, *53*(4), 2220–2228. https://doi.org/10.1021/acs.est.8b05355

Guo, J., Su, T., Chen, D., Wang, J., Li, Z., Lv, Y., et al. (2019). Declining summertime local-scale precipitation frequency over China and the United States, 1981–2012: The disparate roles of aerosols. *Geophysical Research Letters*, *46*(22), 13281–13289. https://doi.org/10.1029/2019gl085442

Krotkov, N. A., McLinden, C. A., Li, C., Lamsal, L. N., Celarier, E. A., Marchenko, S. V., et al. (2016). Aura OMI observations of regional SO2 and NO2 pollution changes from 2005 to 2015. *Atmospheric Chemistry and Physics*, *16*(7), 4605–4629. https://doi.org/10.5194/acp-16-4605-2016

Li, M., Zhang, Q., Kurokawa, J.-i., Woo, J.-H., He, K., Lu, Z., et al. (2017). MIX: A mosaic Asian anthropogenic emission inventory under the international collaboration framework of the MICS-Asia and HTAP. *Atmospheric Chemistry and Physics*, *17*, 935–963. https://doi.org/10.5194/acp-17-935-2017

Li, R., Mei, X., Chen, L., Wang, L., Wang, Z., & Jing, Y. (2020). Long-term (2005–2017) view of atmospheric pollutants in central China using multiple satellite observations. *Remote Sensing*, *12*, 1041. https://doi.org/10.3390/rs12061041

Liu, Y., Hu, C., Zhan, W., Sun, C., Murch, B., & Ma, L. (2018). Identifying industrial heat sources using time-series of the VIIRS Nightfire product with an object-oriented approach. *Remote Sensing of Environment*, *204*, 347–365. https://doi.org/10.1016/j.rse.2017.10.019

Oberschelp, C., Pfister, S., Raptis, C. E., & Hellweg, S. (2019). Global emission hotspots of coal power generation. *Nature Sustainability*, *2*(2), 113–121. https://doi.org/10.1038/s41893-019-0221-6

Qu, Z., Henze, D. K., Capps, S. L., Wang, Y., Xu, X., Wang, J., & Keller, M. (2017). Monthly top-down NOx emissions for China (2005–2012): A hybrid inversion method and trend analysis. *Journal of Geophysical Research: Atmospheres*, *122*(8), 4600–4625. https://doi.org/10.1002/2016jd025852

Schroeder, W., Oliva, P., Giglio, L., & Csiszar, I. A. (2014). The New VIIRS 375 m active fire detection data product: Algorithm description and initial assessment. *Remote Sensing of Environment*, *143*, 85–96. https://doi.org/10.1016/j.rse.2013.12.008

Streets, D. G., Bond, T. C., Carmichael, G. R., Fernandes, S. D., Fu, Q., He, D., et al. (2003). An inventory of gaseous and primary aerosol emissions in Asia in the year 2000. *Journal of Geophysical Research*, *108*(D21), 8809. https://doi.org/10.1029/2002jd003093

Tao, M., Wang, J., Li, R., Chen, L., Xu, X., Wang, L., et al. (2020). Characterization of aerosol type over east Asia by 4.4 km MISR product: First insight and general performance. *Journal of Geophysical Research: Atmosphere*, *125*(13), e2019JD031909. https://doi.org/10.1029/2019jd031909

Wang, Y., Wang, J., Xu, X., Henze, D. K., Qu, Z., & Yang, K. (2020). Inverse modeling of SO2 and NOx emissions over China using multi-sensor satellite data – Part 1: Formulation and sensitivity analysis. *Atmospheric Chemistry and Physics*, *20*(11), 6631–6650. https://doi.org/10.5194/acp-20-6631-2020

Wang, Y., Wang, J., Xu, X., Henze, D. K., Wang, Y., & Qu, Z. (2016). A new approach for monthly updates of anthropogenic sulfur dioxide emissions from space: Application to China and implications for air quality forecasts. *Geophysical Research Letters*, *43*(18), 9931–9938. https://doi.org/10.1002/2016gl070204

Wang, Z., Shao, M., Chen, L., Tao, M., Zhong, L., Chen, D., et al. (2016). Space view of the decadal variation for typical air pollutants in the Pearl River Delta (PRD) region in China. *Frontiers of Environmental Science & Engineering*, *10*(5), 9. https://doi.org/10.1007/s11783-016-0853-y

Zhang, P., Yuan, C., Sun, Q., Liu, A., You, S., Li, X., et al. (2019). Satellite-based detection and characterization of industrial heat sources in China. *Environmental Science & Technology*, *53*, 11031–11042. https://doi.org/10.1021/acs.est.9b02643

Zhang, Q., Streets, D. G., Carmichael, G. R., He, K. B., Huo, H., Kannari, A., et al. (2009). Asian emissions in 2006 for the NASA INTEX-B mission. *Atmospheric Chemistry and Physics*, *9*(14), 5131–5153. https://doi.org/10.5194/acp-9-5131-2009

Zhao, Y., Nielsen, C. P., Lei, Y., McElroy, M. B., & Hao, J. (2011). Quantifying the uncertainties of a bottom-up emission inventory of anthropogenic atmospheric pollutants in China. *Atmospheric Chemistry and Physics*, *11*, 2295–2308. https://doi.org/10.5194/acp-11-2295-2011

Zheng, B., Tong, D., Li, M., Liu, F., Hong, C., Geng, G., et al. (2018). Trends in China's anthropogenic emissions since 2010 as the consequence of clean air actions. *Atmospheric Chemistry and Physics*, *18*(19), 14095–14111. https://doi.org/10.5194/acp-18-14095-2018